COMPARATIVE STUDY OF SUPERHYDROPHILIC AND SUPERHYDROPHOBIC TiO$_2$/EPOXY COATINGS ON AISI 316L STAINLESS STEEL: SURFACE PROPERTIES AND BIOCOMPATIBILITY

PRIMERJAVA SUPERHIDROFILNIH IN SUPERHIDROFOBNIH TiO$_2$/EPOKSI PREVLEK NA NERJAVNEM JEKLU AISI 316L: POVRŠINSKE LASTNOSTI IN BIOKOMPATIBILNOST

Aleksandra Kocijan[1], Marjetka Conradi[1], Matej Hočevar[1], Damjana Drobne[2]

[1]Institute of Metals and Technology, Lepi pot 11, SI-1000 Ljubljana, Slovenia
[2]Biotechnical Faculty, University of Ljubljana, Jamnikarjeva 101, SI-1000 Ljubljana, Slovenia
aleksandra.kocijan@imt.si

TiO$_2$/epoxy coatings were successfully applied to the surface of AISI 316L stainless steel to change the wetting properties, with the aim being to improve the biocompatibility of the superhydrophobic/superhydrophilic surfaces. Contact-angle measurements were used to evaluate the wetting properties of the non-coated, epoxy-coated, as-received TiO$_2$/epoxy-coated and fluoroalkyl-silane (FAS)-TiO$_2$/epoxy-coated substrates. The as-received TiO$_2$/epoxy coating and FAS-TiO$_2$/epoxy coating showed super-hydrophilic and superhydrophobic characteristics, respectively. The average surface roughness (S_a) of the superhydrophobic surface was higher compared to the superhydrophilic surface due to the formation of agglomerates. The biocompatibility evaluated by cell attachment showed that AISI 316L stainless steel with a hydrophilic nature and low S_a is the most favourable surface for bone osteosarcoma cells (MG-63) growth. On the other hand, the two limiting cases of surfaces, superhydrophilic and superhydrophobic coatings with increased roughness compared to AISI 316L, showed lower biocompatibility.

Keywords: stainless steel, epoxy coating, TiO$_2$, wetting properties, biocompatibility

Na površino nerjavnega jekla tipa AISI 316L smo uspešno nanesli TiO$_2$/epoksi prevleke z namenom regulacije omočitvenih lastnosti, ki vplivajo na izboljšanje biokompatibilnosti superhidrofobnih/superhidrofilnih površin. Z meritvami kontaktnih kotov smo določili omočitvene lastnosti čiste jeklene površine ter jeklene površine prevlečene z epoksidno smolo, s TiO$_2$/epoksi prevleko in fluoroalkilsilan (FAS)-TiO$_2$/epoksi prevleko. TiO$_2$/epoksi prevleka je pokazala superhidrofilno, FAS-TiO$_2$/epoksi prevleka superhidrofobno naravo. Povprečna hrapavost površine (S_a) superhidrofobne površine je bila višja kot na superhidrofilni površini zaradi opažene tvorbe aglomeratov. Analiza biokompatibilnosti je pokazala, da je nerjavno jeklo AISI 316L s hidrofilno naravo in nizko S_a najprimernejša površina za rast kostnega osteosarkoma (MG-63). Po drugi strani pa sta oba mejna primera prevlek s superhidrofilno in superhidrofobno naravo z večjo hrapavostjo v primerjavi z AISI 316L, pokazala manjšo stopnjo biokompatibilnosti.

Ključne besede: nerjavno jeklo, epoksi prevleka, TiO$_2$, omočitvene lastnosti, biokompatibilnost

1 INTRODUCTION

The major issues in the biomedical applications of stainless steels are related to understanding the relationship between the surface properties of the material and the cellular responses, accompanied by the risk of microbial infections.[1] The interaction of nanoscale surface topographies with cells was proven to play a crucial role in the biocompatibility of implants.[2] Various nanoscale surface modifications have been proposed in order to enhance the biocompatibility and antibacterial activity of medical implants.[3] Epoxy resins are widely used as long-term protective coatings for stainless steels in various applications.[4,5] However, their susceptibility to abrasion[6] and poor resistance to crack propagation, due to a highly cross-linked structure[7], have inspired major research efforts to develop improved nanostructured composite coatings by adding various inorganic nano-

fillers such as silica[8–10] or TiO$_2$.[11,12] The unique surface properties and high surface energy of the nanomaterials provide additional available sites for protein adsorption, which enhances the interaction between the cells and the implant.[13] K. Webb et al.[1] reported that hydrophilic surfaces promote significantly greater cell attachment, cell spreading, and cytoskeletal organization compared to hydrophobic surfaces. D. S. Kommireddy et al.[14] studied super-hydrophilic TiO$_2$ nanoparticle thin films prepared by using a layer-by-layer nano-assembly method. The biocompatibility of the coating was demonstrated by the successful attachment of human dermal fibroblast cell culture. K. Mehrabi et al.[15] reported that the presence of nanoscale features on the surface of implants enhanced the growth and attachment of osteoblast bone-forming cells. Such enhancement is due to an increase in the surface area that provides more area for the cell–substrate interaction, more surface energy,

more protein adsorption, integrin clustering, and as a result, higher cell adhesion. K. Anselme et al.[16] reported on the influence of topography, chemistry and surface energy on osteoblast/material interaction. These surface characteristics determine how the biological molecules will adsorb to the surface and more particularly determine the orientation of the adsorbed molecules. K. Das et al.[17] showed that osteoblast proliferation was significantly higher on an anodized nanotube surface. The surface properties changed with the emergence of nanoscale morphology. The higher nanometer-scale roughness, low contact angle and high surface energy in the nanoporous surface enhanced the osteoblast-material interactions. A growing number of studies report that a topographical modification of the cell-substrate interface is a significant regulator of cellular adhesion and function.[18] The future surface modifications will go in the direction of controlling cellular interactions, with the aim being to enhance tissue regeneration, to regulate cellular adhesion and their differentiation.[19]

In the present study we focus on the biocompatibility of epoxy coatings on AISI 316L stainless steel by adding as-received and surface-modified TiO₂ nanoparticles with an emphasis on tuning the wetting properties between the two limiting cases, i.e., superhydrophobic/superhydrophilic coatings. The surface morphology, surface roughness, contact-angle and surface energy, as well as the biocompatibility of as-received and surface-modified TiO₂/epoxy coatings on the AISI 316L stainless steel, were evaluated and compared with the characteristics of bare and epoxy-coated AISI 316L stainless steel.

2 MATERIALS AND METHODS

Materials. • Austenitic stainless steel AISI 316L (17 % Cr, 10 % Ni, 2.1 % Mo, 1.4 % Mn, 0.38 % Si, 0.041 % P, 0.021 % C, < 0.005 % S in mass fraction) was used as the substrate.

A two-component USP Class VI biocompatible epoxy EPO-TEK 302-3M (EPOXY TECHNOLOGY, Inc.) was mixed in the % of mass fractions ratio 100:45. TiO₂ nanoparticles with mean diameters of 30 nm were provided by Cinkarna Celje, whereas the 300-nm particles were supplied by US Research Nanomaterials, Inc.

Surface modification of TiO₂. • The TiO₂ particles were functionalized in 1 % of volume fractions of fluoroalkylsilane or FAS17 ($C_{16}H_{19}F_{17}O_3Si$) ethanol solution. The solution was shaken for a few minutes and left overnight prior to use in the experiments.

Steel substrate preparation. • The steel sheet with a thickness of 1.5 mm was cut into discs of 25-mm diameter. The steel discs were grinded mechanically with SiC emery paper (up to 4000 grit), diamond polished (up to 1 μm), ultrasonically cleaned with ethanol and dried in warm air.

Coating preparation. • Prior to the TiO₂ nanoparticle adsorption, the diamond-polished AISI 316L substrate was spin-coated with a 300-nm layer of epoxy (as determined by ellipsometry) and then cured for 1 h at 70 °C and post-cured at 150 °C for another hour. [20] We decided on a thin base epoxy layer to improve the TiO₂ nanoparticle adhesion as the oxide layer growing on the surface of the clean AISI 316L substrate prevents adhesion and is very difficult to remove. The nanoparticles were further applied to the epoxy-coated AISI 316L surface by spin-coating 20 μL of 3 % of mass fractions of TiO₂ nanoparticle ethanol solution. We consecutively applied three deposits of dual-size, dual-layer coating consisting of 30-nm and 300-nm FAS-TiO₂ nanoparticles. The coating was then dried in an oven for approximately 30 min at 100 °C. The same procedure was repeated with the as-received, non-functionalized TiO₂ nanoparticles.

Surface roughness. • An optical 3D metrology system, Alicona Infinite Focus (Alicona Imaging GmbH), was employed for the surface-roughness analysis. At least three measurements per sample were performed at a magnification of 20× with a lateral resolution of 0.9 μm and a vertical resolution of about 50 nm. IF-Measure-Suite (Version 5.1) software was used for the roughness analysis. The software offers the possibility to calculate the average surface roughness, S_a, for each sample, based on the general surface-roughness Equation (1):

$$Sa = \frac{1}{L_x}\frac{1}{L_y}\int\limits_0^{L_x}\int\limits_0^{L_y}|z(x,y)|\mathrm{d}x\mathrm{d}y \qquad (1)$$

where L_x and L_y are the acquisition lengths of the surface in the x and y directions and $z(x,y)$ is the height. The size of the analyzed area was 714×542 μm². To level the profile, corrections were made to exclude the general geometrical shape and possible measurement-induced misfits.

Contact-angle measurements. • The static contact-angle measurements of water (W) on a clean AISI 316L diamond-polished sample, on the epoxy-coated AISI 316L substrate, on the TiO₂/epoxy-coated AISI 316L substrate and on the FAS-TiO₂/epoxy-coated AISI 316L substrate were performed using a surface-energy evaluation system (Advex Instruments s.r.o.). Liquid drops of 5 μL were deposited on different spots of the substrates to avoid the influence of roughness and gravity on the shape of the drop. The drop contour was analysed from the image of the deposited liquid drop on the surface and the contact angle was determined using Young-Laplace fitting. To minimize the errors due to roughness and heterogeneity, the average values of the contact angles of the drop were calculated approximately 30 s after the deposition from at least five measurements on the studied coated steel. All the contact-angle measurements were carried out at 20 °C and ambient humidity. As the contact angles were only available for water, an

equation-of-state approach[21] was used to calculate the corresponding surface energies.

Scanning Electron Microscopy (SEM). • SEM analysis using a FE-SEM JEOL JSM-6500F was employed to investigate the surface morphology of the coatings as well as the morphology and distribution of the attached cells after a biological evaluation. The samples were sputtered with gold prior to the imaging. The thickness of the coatings was determined by cross-section SEM images. The specimen cross-sections for SEM were prepared using a JEOL Cross Section Polisher SM-09010.

Biocompatibility evaluation. • Fast-growing bone osteosarcoma cells (MG-63; (ATCC® CRL-1427™) were used for the assessment of cytocompatibility/biocompatibility on sterilized epoxy, epoxy-TiO₂ and stainless-steel samples (given/obtained by the Krasteva Institute of Biophysics and Biomedical Engineering, Bulgarian Academy of Sciences, Sofia, Bulgaria). MG63 cells were cultured under controlled conditions (37 °C, 5 % CO_2, high humidity) in Dulbecco's modified Eagle's medium (DMEM), supplemented with etal bovine serum (FBS; 10 %, v/v) and 4-mM L-glutamine (all the reagents were purchased from Sigma-Aldrich, Steinheim, Germany). Cells were routinely subcultured once a week or when they reached 65–70 % confluence. Before harvesting with Trypsin-0.25 % EDTA (Sigma-Aldrich, Steinheim, Germany) for approximately 10 minutes at 37 °C, the cells were washed three times with Phosphate Buffered Saline without Ca^{2+} and Mg^{2+} (PBS; Sigma-Aldrich, Steinheim, Germany). The cells were then re-suspended in the growth medium, centrifuged at 200 g for 5 min, and plated at a seeding density of $3 × 10^4$ cells/cm² in 6-well plates (*Sigma-Aldrich, TPP ®*, Steinheim, Germany) containing epoxy, epoxy-TiO₂ and stainless-steel samples, all in 3 mL of growth medium ($27 × 10^4$ cells/well) and incubated for 24 h under controlled laboratory conditions (5 % CO_2/95 % air at 37 °C). Then, the cells were further processed for SEM fixation. After 24 h of incubation, the cell-culture medium was removed, cells were washed three times with PBS and fixed for 24 h at 4 °C using a modified Karnovsky fixative, composed of 2.5 % glutaraldehyde (SPI Supplies, West Chester, PA, USA) and 0.4 % paraformaldehyde (Merck KGaA, Darmstadt, Germany) in a 0.1-M Na-phosphate buffer (NaH_2PO_4 $2·H_2O$ and Na_2HPO_4 $2·H_2O$; all the chemicals from Merck KGaA, Darmstadt, Germany). Then the samples were washed in the buffer for 3 × 10 min and post-fixated with 1 % osmium tetroxide (OsO_4) (SPI Supplies, West Chester, PA, USA; 1 × 60 min), followed by washing in the buffer for 3 × 10 min. The samples were dehydrated through an alcohol gradient (30–100 %) (EtOH; Merck KGaA, Darmstadt, Germany) with each step lasting 10 min. Further dehydration steps were conducted with a mixture of Hexamethyldisiloxane (HMDS; SPI Supplies, West Chester, PA, USA) and absolute EtOH (1:1; v/v; 10 min), 3:1 (HMDS: absolute EtOH, v/v; 10 min) and absolute HMDS (10 min) and HMDS (2 h), which was finally left to evaporate. The SEM was used to visualize the distribution, the number and the shape of the attached M63 cells.

Optical Microscopy. • Optical microscope Microphot FXA (Nikon, Japan) with an Olympus DP73 camera was used to visualise the number and the distribution of the attached MG63 cells. Twenty images from different fields of view were randomly taken per sample, and each of the four different surfaces was investigated in triplicate. The software program Stream Motion was used to quantify (the percentage of coverage) the number and distribution of adhered cells and the results are shown as the arithmetic mean ± the standard deviation. The difference in the median-measured parameters in the exposed and unexposed groups was tested with the non-parametric Mann-Whitney U test. All the calculations were performed with Statgraphics Plus 4.0. All the data were
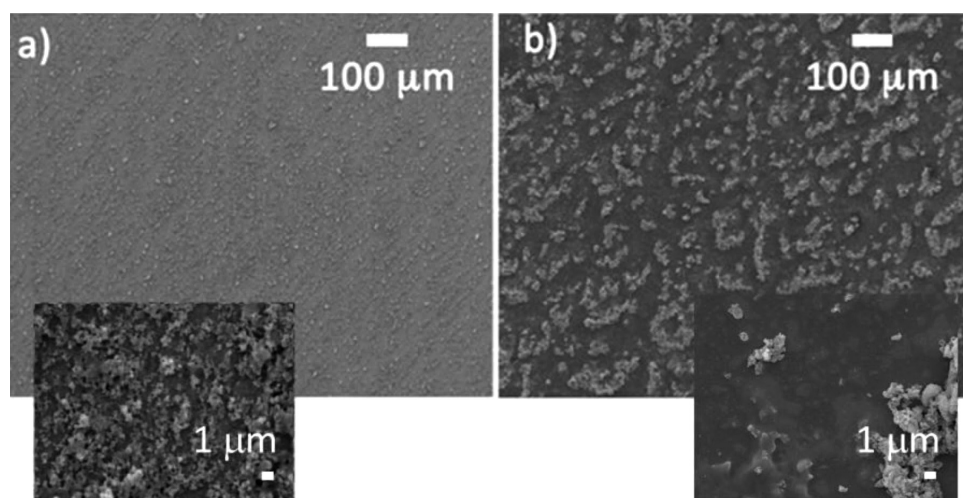

Figure 1: SEM images of surface morphology of: a) as-received TiO₂/epoxy coatings on AISI 316L stainless steel and b) FAS-TiO₂/ epoxy coatings on AISI 316L stainless steel; the zoomed-out insets show the significant morphology difference between the two coatings

submitted for an analysis of variance (ANOVA) and Duncan's multiple range test, where appropriate.

3 RESULTS AND DISCUSSION

3.1 Surface properties

The morphology of the as-received TiO$_2$/epoxy and FAS-TiO$_2$/epoxy coatings was compared by SEM imaging (**Figure 1**). The SEM images reveal a difference in the morphology between the two coatings, which is mostly reflected in the different length scales of the average size of the nanoparticle agglomerates. FAS functionalization apparently does not homogenize the particle distribution as the formation of large agglomerates up to a few tens of microns is observed during the deposition of the FAS-TiO$_2$ nanoparticles (**Figure 1b**). In contrast, in the as-received TiO$_2$ nanoparticle coatings, the nanoparticles are more finely dispersed and agglomerates of the order of only a few microns are observed (**Figure 1a**). This is confirmed by the average surface-roughness measurements, which are reported in **Table 1**.

To analyse the surface wettability, we performed five static contact-angle measurements with water (W) on different spots all over the sample and to calculate the corresponding surface energy. The average surface-roughness parameter was used to evaluate the morphology difference between the two coatings under investigation.

Table 1: Surface properties of diamond-polished AISI 316L, epoxy coated AISI 316L and TiO$_2$ coatings prepared from FAS-TiO$_2$ and as-received TiO$_2$ nanoparticles: static water contact angles (θ^W), the corresponding surface energies (γ) and the average surface roughness (S_a). All data are reported as mean ± standard deviation (*n*=5)

Substrate	q^W (°)	g (mN/m)	S_a (nm)
0065 AISI 316L	57±1	49±5	31±4
epoxy coated AISI 316L	71±1	41±3	50±5
TiO$_2$/epoxy coated AISI 316L	< 5	72±7	423±20
FAS-TiO$_2$/epoxy coated AISI 316L	160±3	0.24±0.02	618±30

With the contact-angle measurements it was confirmed that we were able to synthesise two limiting cases of coatings concerning their wetting characteristics. The FAS-TiO$_2$/epoxy coating was superhydrophobic and the as-received TiO$_2$/epoxy coating was superhydrophilic.

As the contact angles were only available for water, an equation-of-state approach[21,22] was used to calculate the surface energies with the Equation (2):

$$\cos\theta = -1 + 2\sqrt{\frac{\gamma_s}{\gamma_1}}e^{-b(\gamma_s - \gamma_1)^2}$$ (2)

For a given value of the surface tension of a probe liquid γ_1 (i.e., for water γ_1 = 72.8 mN/m)[23] and θ^W measured on the same solid surface, the constant β and the solid surface-tension γ_s values were determined using the least-squares analysis technique. For the fitting with

equation (2), a literature value of β = 0.0001234 (mJ/m^2)$^{-2}$ was used, as weighted for a variety of solid surfaces.[21,22] The calculated values of the solid surface energy are listed in **Table 1** and confirm the two limits of the superhydrophobic and the superhydrophilic surface.

The measured average surface roughness indicates a slight difference in the average surface-roughness parameter S_a (**Table 1**) between the FAS-TiO$_2$/epoxy and the as-received TiO$_2$/epoxy coatings, which is in agreement with the surface morphology evaluated with the SEM. The rougher FAS-TiO$_2$/epoxy surface is covered with large agglomerates, whereas in the as-received TiO$_2$/epoxy coatings the nanoparticles are more finely dispersed, resulting in a reduced roughness (**Table 1** and **Figure 1**).

As a reference we also measured the contact angles, surface energies and average surface roughness on diamond-polished AISI 316L and epoxy-coated AISI 316L.

3.2 Biocompatibility

Biomaterials are never truly inert, but they are biotolerable to different degrees. The cyto-compatibility of a material can be assessed *in vitro* by observing the growth and differentiation that is manifested by the cellular density and morphological characteristics of cells grown on specific surfaces. After the initial cell attachment, the cells are transformed with time: a decrease in the cell widths and an increase in the cell lengths. The time dependence of the cell morphological transition could be explained in terms of the re-organization of focal contacts and the intracellular cytoskeleton.[24]

The cytocompatibility/biocompatibility of the AISI 316L stainless steel, the epoxy-coated AISI 316L, the as-received TiO$_2$/epoxy coating on AISI 316L and the
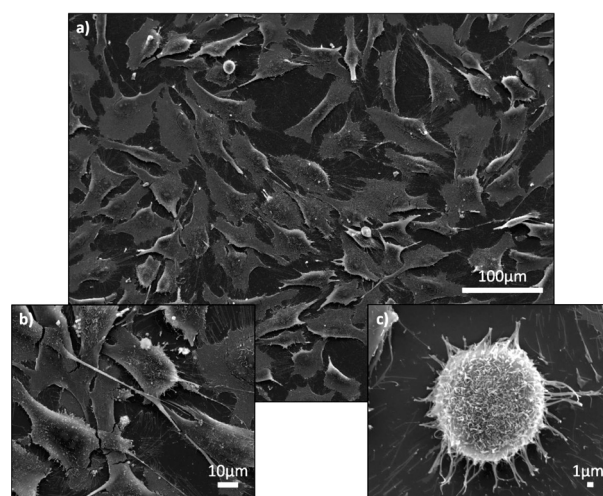

Figure 2: SEM images of MG63 cells attached to AISI 316L stainless-steel surface: a) distribution, attachment pattern and shape of the cells, b) flatten cells with one or two longer protrusions, c) round-shaped cell has many outgrowths in various shapes, mostly tubular or vesicular structures of up to 2 μm in size
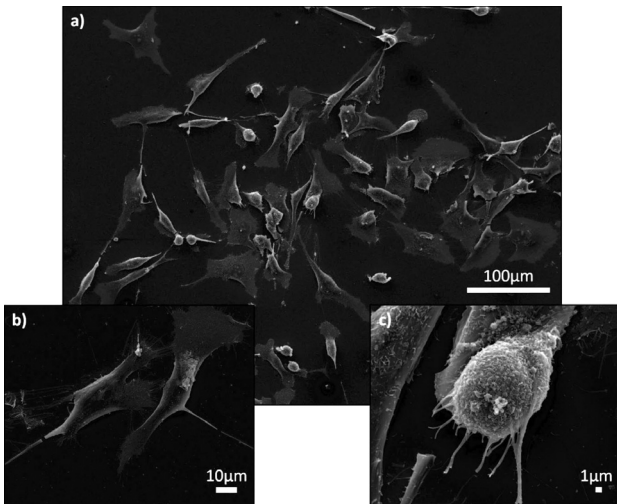
Figure 3: SEM images of MG63 cells attached to epoxy-coated AISI 316L surface: a) distribution, attachment pattern and shape of the cells, b) cells with flat and cuboidal to elongated parts, with numerous delicate cellular filamentous extensions, c) round-shaped part of the cell
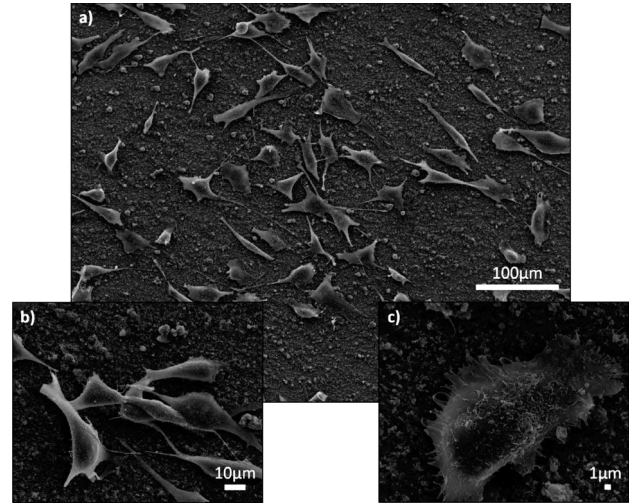

Figure 4: SEM images of MG63 cells attached to hydrophilic as-received TiO₂/epoxy-coated AISI 316L surface: a) distribution, attachment pattern and shape of the cells, b) cells are predominantly rounded and tightly attached to the surface with only one very long filamentous protrusion, c) magnified part of the cell

FAS-TiO₂/epoxy coating on AISI 316L were evaluated using the attachment of bone osteosarcoma cells.

In the case of bare AISI 316L stainless steel (**Figure 2**), the cells were randomly distributed over the surface of the specimens and half of the surface was covered with attached cells (**Table 2**). The majority of the cells were 50–100 μm. The morphology of the cells was 95 % polygonal, with less than 5 % being round shaped. They differed in terms of size and the degree of flatness. The flatter the cell, the larger the area they were occupying. Most of the cells had one or two longer protrusions. Some cells had one very long protrusion, which was even longer than the entire cell and could reach up to 100 μm or even more. The surface morphology of the flat part was less structured with rare tubular protrusions. The round cells or rounded parts of the flat cells had many outgrowths in various shapes, but they were mostly tubular or vesicular structures of up to 2 μm in size. In some round-shaped cells the vesicular outgrowths prevailed. The round-shaped cells were, in most cases, not attached to the surface by filamentous expansions, but there were some exceptions, which appeared to be a transitional phase.

Table 2: Cell attachment after 24 h of exposure expressed as a percentage of the covered surface; all data are reported as mean ± standard deviation (*n*=5)

Material	Cell attachment (% of covered surface)
AISI 316L	55±9
Epoxy coated AISI 316L	20±6
TiO₂/epoxy coated AISI 316L	12±2
FAS-TiO₂/epoxy coated AISI 316L	7±2

In the case of the epoxy-coated AISI 316L samples (**Figure 3**), the adhesion pattern was similar to the bare AISI 316L stainless steel. However, the cells were more randomly attached over the surface and the percentage of the covered surface was two times lower (**Table 2**). The size of the cells was up to 100 μm along the longest axis. Most of the cells (up to 90 %) had two morphological features. One part of the cell was flat, cuboidal-to-elongated in one axis, with numerous delicate cellular filamentous extensions attached to the material surface. Some cells had one very long filamentous protrusion. The other part of the same cell was round shaped and 10–30 μm in diameter. This region was higher in the z axis, rounded, with edges detached from the surface. The surface morphology of the round and flat parts of the cell was also significantly different. The surface of the flat part was less structured with rare tubular protrusions. The upper surface of the round part of a cell had many outgrowths in various shapes, ranging from tubular, lamellar to vesicular structures up to 2 μm in size.

In the case of the superhydrophilic as-received TiO₂/epoxy coating on AISI 316L (**Figure 4**), the cells were distributed more randomly and formed cluster patterns across the surface, compared to the AISI 316L and epoxy-coated AISI 316L samples. The cells covered 8 % less surface than observed on the epoxy-coated AISI 316L samples (**Table 2**). The majority of the cells measured approximately 50 μm in diameter. Most of the cells (95 %) were elongated, spindle-shaped. Some (less than 5 %) were round shaped, but not completely rounded. No cells or parts of them were flat and tightly attached to the surface by delicate filamentous protrusions. Most of the cells had one very long filamentous protrusion, sometimes exceeding the size of the cells. Occasionally, the protrusions of different cells were tightly connected. The round cells or parts of the cells were more structured than the flatter parts of the cell. The cell surface was covered with mostly tubular protru-
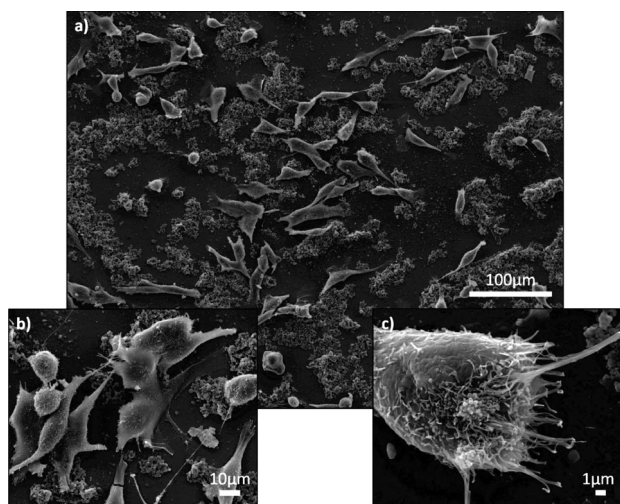
Figure 5: SEM images of MG63 cells attached to hydrophobic FAS-TiO$_2$/epoxy-coated AISI 316L samples: a) distribution, attachment pattern and shape of the cells at lower magnification, b) cells are spindle-shaped with rounded central part and they exhibit different degrees of roundness, c) magnified part of the cell

sions of different densities. Vesicles apparently adsorbed to the surface were also observed.

In the case of the superhydrophobic FAS-TiO$_2$/epoxy coating on AISI 316L (**Figure 5**), the cells attached to the surface exhibited a similar pattern of attachment as in the case of the as-received TiO$_2$/epoxy-coated AISI 316L samples. The percentage of covered surface with cells is the lowest of all the compared samples: only 7 % of the surface was covered by cells (**Table 2**). The cells preferred to grow on flat surfaces with fewer TiO$_2$ particles. However, they were also found to overgrow the TiO$_2$ particles deposited on the flat surface. The majority of the cells measured approximately 30–50 μm in diameter. Most of the cells were spindle-shaped with a rounded central part; they exhibited different degrees of roundness. Approximately 10 % of the cells were irregularly round shaped. Some spindle-like cells had a stocky protrusion that was strongly attached to the surface by delicate filamentous protrusions. Some cells had one or two very long filamentous protrusions up to 200 μm. The protrusions of the different cells were occasionally connected. The round cells or parts of the cells were more structured than the flatter parts of the cell. The cell surface was covered with mostly tubular protrusions of different densities. Vesicles apparently adsorbed to the surface were also observed.

Several studies have indicated superior cell attachment and cell spreading on (super)hydrophilic surfaces compared to hydrophobic surfaces.[1,14] We evaluated two limiting cases of surface wettability, i.e., superhydrophobic vs. superhydrophilic coatings, and the results were comparable with the literature data.[1,14] This study shows that both surface topographical and chemical cues modulate the cell morphology and spreading. We observed a variability in cell abundance, size, shape, number, shape and size of the protrusions as well as the

surface structures of the cells. We found that different surface characteristics significantly modulated the morphological features of cells and their abundance. The results indicated improved cell adhesion on the bare AISI 316L stainless steel compared to the superhydrophobic/superhydrophilic coatings. This suggests that surfaces with moderate hydrophilic nature (i.e., contact angles around 50–60°) are more appropriate for proposed applications. In addition to the appropriate wetting properties, we have shown that the low surface roughness also plays a crucial role in improving the cell adhesion. On AISI 316L surface, the cells appeared flattened and were able to maintain their osteoblastic morphology. The cells were attached to the material surface by numerous fine filamentous extensions. This is in line with the literature data, which report that cell adhesion is generally better on hydrophilic surfaces.[25] The cell growth indicated by a portion of covered material was less pronounced on the other three materials, especially on the superhydrophobic surface. However, all three materials exhibited some unique characteristics that were manifested in the different morphological responses of the cells. Optimal tissue regeneration can be induced only by the selective cell adhesion/activation for cells of interest, but not for others.

4 CONCLUSIONS

In our work we were able to significantly influence the wetting properties and biocompatibility of coated AISI 316L stainless steel by altering the surface topographical and chemical features. Superhydrophobic FAS-TiO$_2$/epoxy and superhydrophilic as-received TiO$_2$/epoxy coatings were successfully fabricated, resulting not only in opposite wetting characteristics but also in different average surface-roughness properties. This was reflected in the formation of larger agglomerates in the FAS-TiO$_2$/epoxy coating, making the superhydrophobic surface more rough compared to the superhydrophilic surface. The biological evaluation showed a significant variation in the cell abundance, size and shape as well as the surface structure of the cells. The results showed that AISI 316L stainless steel is the most favourable surface for bone osteosarcoma cells (MG-63), followed by the epoxy, superhydrophilic and superhydrophobic coatings, respectively.

The information provided in our work shows that the four applied surfaces interact very differently with bone osteosarcoma cells in terms of attachment pattern and could thus be used for different purposes where low or high attachment intensity is required. The results presented in this paper can inspire new strategies for the preparation of titanium dioxide nanoparticle surfaces for biomedical applications.

Acknowledgments

5 REFERENCES

[1] K. Webb, V. Hlady, P. A. Tresco, Relative importance of surface wettability and charged functional groups on NIH 3T3 fibroblast attachment, spreading, and cytoskeletal organization, Journal of Biomedical Materials Research, 41 (**1998**) 3, 422–430

[2] M.-Y. Lan, C.-P. Liu, H.-H. Huang, S.-W. Lee, Both Enhanced Biocompatibility and Antibacterial Activity in Ag-Decorated TiO2 Nanotubes, Plos One, 8(10) (2013)

[3] L. Visai, L. De Nardo, C. Punta, L. Melone, A. Cigada, M. Imbriani, C.R. Arciola, Titanium oxide antibacterial surfaces in biomedical devices, Int. J. Artif. Organs., 34 (**2011**), 929–946

[4] F. Galliano, D. Landolt, Evaluation of corrosion protection properties of additives for waterborne epoxy coatings on steel, Progress in Organic Coatings, 44 (**2002**) 3, 217–225

[5] F. W. Liu, M. X. Yin, B. Y. Xiong, F. Zheng, W. F. Mao, Z. Chen, C. Q. He, X. P. Zhao, P.F. Fang, Evolution of microstructure of epoxy coating during UV degradation progress studied by slow positron annihilation spectroscopy and electrochemical impedance spectroscopy, Electrochimica Acta, 133 (**2014**), 283–293

[6] B. Wetzel, F. Haupert, M. Q. Zhang, Epoxy nanocomposites with high mechanical and tribological performance, Composites Science and Technology 63 (**2003**) 14, 2055–2067

[7] S. Yamini, R. J. Young, Stability of crack-propagation in epoxy-resins, Polymer 18 (**1977**) 10, 1075–1080

[8] M. Conradi, M. Zorko, A. Kocijan, I. Verpoest, Mechanical properties of epoxy composites reinforced with a low volume fraction of nanosilica fillers, Materials Chemistry and Physics, 137 (**2013**) 3, 910–915

[9] M. Conradi, A. Kocijan, D. Kek-Merl, M. Zorko, I. Verpoest, Mechanical and anticorrosion properties of nanosilica-filled epoxy-resin composite coatings, Applied Surface Science, 292 (**2014**), 432–437

[10] M. Conradi, A. Kocijan, M. Zorko, I. Verpoest, Damage resistance and anticorrosion properties of nanosilica-filled epoxy-resin composite coatings, Progress in Organic Coatings, 80 (**2015**), 20–26

[11] H. A. Al-Turaif, Effect of nano TiO$_2$ particle size on mechanical properties of cured epoxy resin, Progress in Organic Coatings, 69 (**2010**) 3, 241–246

[12] A. Kubacka, M. S. Diez, D. Rojo, R. Bargiela, S. Ciordia, I. Zapico, J. P. Albar, C. Barbas, V. A. P. M. dos Santos, M. Fernandez-Garcia, M. Ferrer, Understanding the antimicrobial mechanism of TiO$_2$-based nanocomposite films in a pathogenic bacterium, Scientific Reports, 4 (**2014**)

[13] A. Simchi, E. Tamjid, F. Pishbin, A. R. Boccaccini, Recent progress in inorganic and composite coatings with bactericidal capability for orthopaedic applications, Nanomedicine-Nanotechnology Biology and Medicine, 7 (**2011**) 1, 22–39

[14] D. S. Kommireddy, A. A. Patel, T. G. Shutava, D. K. Mills, Y. M. Lvov, Layer-by-layer assembly of TiO$_2$ nanoparticles for stable hydrophilic biocompatible coatings, Journal of Nanoscience and Nanotechnology, 5 (**2005**) 7, 1081–1087

[15] K. Mehrabi, H. Bahmanpour, A. Shokuhfar, A. Kneissl, Influence of chemical composition and manufacturing conditions on properties of NiTi shape memory alloys, Materials Science and Engineering a-Structural Materials Properties Microstructure and Processing, 481 (**2008**), 693–696

[16] K. Anselme, Osteoblast adhesion on biomaterials, Biomaterials, 21 (**2000**) 7, 667–681

[17] K. Das, S. Bose, A. Bandyopadhyay, TiO$_2$ nanotubes on Ti: Influence of nanoscale morphology on bone cell-materials interaction, Journal of Biomedical Materials Research Part A 90A (**2009**) 1, 225–237

[18] I. Junkar, M. Kulkarni, B. Drasler, N. Rugelj, N. Recek, D. Drobne, J. Kovac, P. Humpolicek, A. Iglic, M. Mozetic, Enhanced biocompatibility of TiO$_2$ surfaces by highly reactive plasma, Journal of Physics D-Applied Physics, 49 (**2016**) 24

[19] W.-B. Tsai, Y.-C. Ting, J.-Y. Yang, J.-Y. Lai, H.-L. Liu, Fibronectin modulates the morphology of osteoblast-like cells (MG-63) on nano-grooved substrates, Journal of Materials Science-Materials in Medicine, 20 (**2009**) 6, 1367–1378

[20] M. Conradi, G. Intihar, M. Zorko, Mechanical and wetting properties of nanosilica/epdxy-coated stainless steel, Mater. Tehnol., 49 (**2015**) 4, 613–618

[21] D. Li, A. W. Neumann, A reformulation of the equation of state for interfacial-tensions, Journal of Colloid and Interface Science, 137 (**1990**) 1, 304–307

[22] D. Y. Kwok, A. W. Neumann, Contact angle measurement and contact angle interpretation, Advances in Colloid and Interface Science, 81 (**1999**) 3, 167–249

[23] Y. Y. Yu, C. Y. Chen, W. C. Chen, Synthesis and characterization of organic – inorganic hybrid thin films from poly(acrylic) and mono-dispersed colloidal silica, Polymer, 44 (**2003**) 3, 593–601

[24] C. A. Mullen, T. J. Vaughan, M. C. Voisin, M. A. Brennan, P. Layrolle, L. M. McNamara, Cell morphology and focal adhesion location alters internal cell stress, Journal of the Royal Society Interface 11 (**2014**) 101

[25] G. Altankov, T. Groth, Reorganization of substratum-bound fibronectin on hydrophilic and hydrophobic materials is related to biocompatibility, Journal of Materials Science-Materials in Medicine, 5 (**1994**) 9–10, 732–737